25th ABCM International Congress of Mechanical Engineering
October 20-25, 2019, Uberlândia, MG, Brazil

COB-2019-2101
DESIGN AND EXPERIMENTAL VALIDATION OF DIGITAL SYNTHETIC IMPEDANCES FOR VIBRATION CONTROL ON ELECTROMECHANICALY COUPLED SYSTEMS

Tarcisio Marineli Pereira Silva
Marcel Araujo Clementino
Carlos De Marqui Jr
Sao Carlos School of Engineering, University of Sao Paulo, Avenida Trabalhador Sao-carlense, São Carlos - SP
tarcismarinelli@hotmail.com, marcelclementino@usp.br, demarqui@sc.usp.br

Abstract. *Piezoelectric materials have been widely used as actuators for vibration control in the past decades. However, most authors consider only analog circuits connected to the terminals of the piezoelectric material while ignoring the use of digital components (such as micro controller, arduinos, etc). In this work, we explore the use of these digital devices associated with piezoelectric elements in order to reduce vibrations on a host structure. Piezoelectric circuits using digital devices require reduced number of electric components (compared to fully analog circuitry approaches), allow enhanced manipulation of piezoelectric voltage and current output and also paves the way to more intelligent systems with adaptive capabilities. This paper explores the theory of digital shunts and presents a numerical model using a Matlab-Simulink capable of representing an electromechanical systems associated with a micro-controller. Numerical results are presented in frequency domain and experimental results are carried out for validation of the numerical model.*

Keywords: *Piezoelectric material, Vibration control, digital devices*

1. INTRODUCTION

In the past decades, piezoelectric materials have been investigated as an alternative technique for controlling undesired vibrations on a large variety of mechanical structures. Piezoelectric materials present a coupling between mechanical forces and electrical fields, meaning that these materials strain when exposed to a voltage and, conversely, produce an electrical voltage when strained (Moheimani S.O.R., 2003). Due to this coupling, mechanical energy can be extracted from the structure and dissipated in an electrical impedance, thus reducing vibrations. The main advantages of using piezoelectric materials consist of lower weight penalty, lower volume and ease to handle when compared to some of the traditional methods for vibration control.

The proper design of the electrical impedance plays a fundamental role in reducing vibration of an electromechanical system. Passive impedances, such as resistive, capacitive and inductive circuits were extensively investigated in the literature. Uchino and Ishii (1988) demonstrated that a resistive shunt has an analogous effect to constraint layer damping treatments on the structure. Capacitive shunts (Lesieutre, 1998) provide small changes in structural stiffness with changing external capacitance but does not modify damping. Forward (1979) investigated an inductive circuit and showed that the inductor cancels the internal piezoelectric capacitance, resulting in an undamped dynamic vibration absorber effect. Furthermore, by combining a resistor and an inductor (in series as explored by Hagood and Von Flotow (1991) or in parallel as showed by Wu (1996)), one obtain the effect of a damped dynamic vibration absorber (as an electromechanical analogue of the well-known Den Hartog vibration absorber). Among passive impedance, resistive-inductive (RL) shunt circuits (series/parallel) have received most attention for presenting greater vibration attenuation. Nonetheless, several issues with passive impedances have been reported, such as narrow frequency bandwidth effectiveness and the requirement of large inductances for the RL cases.

To overcome these limitations, several researchers have also explored different types of nonlinear piezoelectric shunt circuits (providing a nonlinear impedance for the piezoelement) to enhance the vibration suppression bandwidth of piezoelectric absorbers and reduce the inductances required. In the early 2000's, Richard *et al.* (1999, 2000); Clark (2000); Guyomar *et al.* (2000); Corr and Clark (2002) developed the Synchronized Switching Damping (SSD) techniques, which consist of including an electrical switch in series with the piezoelectric material. The switch is synchronously driven with the structure motion and, during short periods, the switch connects the piezoelement to a circuit which can be either a simple short circuit (SSDS) or a small inductor (SSDI). Due to this process, a voltage magnification is obtained and a phase-agreement between the structural velocity and the piezoelectric voltage occurs, increasing the energy dissipated by

the piezoelectric material when compared to passive techniques.

Although several techniques have been successfully developed for piezoelectric vibration control, most of them rely on analog circuitry to implement the control method. Thus, in order to implement each technique one should build a different analog circuit. In this sense, some researchers (Matten *et al.*, 2014; Moheimani S.O.R., 2003; Nečásek *et al.*, 2016) started to explore the use of digital platforms connected to piezoelectric materials to reduce vibrations, naming this technique digital shunts. Digital shunts are able to create equivalent electrical impedance across the electrodes of a piezoelectric element. Electrical impedance establishes a relation between the current and the voltage of the piezoelectric material, which is is computed by a digital device with a recurrent equation. As main advantages, digital shunts require reduced number of electric components (compared to fully analog circuitry approaches), present very low threshold (ideally with zero threshold, since no semi-conductive components are required, but some threshold issues are observed in experimental tests) and also allow enhanced manipulation of piezoelectric voltage/current output, which provides adaptive capabilities to the system. In addition, they allow implementation of different techniques without performing changes in the circuit topology since modifications are carried out via software programming inside the microcontroller unit (MCU). A disadvantage of the digital approach, however, relies on the fact that its operational frequency bandwidth is restricted to a lower bandwidth if compared to analog circuits (due to limited processing performance of the MCU). Moreover, the digital platform often requires external power source to operate and such dependence difficult their application to self-powered systems. Despite these drawbacks, the digital shunts pave the way to more intelligent systems with adaptive capabilities.

This paper presents a practical association of digital devices to piezoelectric materials that requires low-cost electrical components and free software. Through this digital interface, the impedances of the resistive, resistive-inductive and SSDI techniques will be reproduced across the electrodes of the piezoelectric material. Since the impedance is created via software, no changes are required in the circuitry topology. This paper presents a numerical model of the digital shunt in Matlab-Simulink capable of simulating both an electromechanical coupled system as well as an MCU. In order to validate numerical results, experimental tests are conducted and results are compared with numerical predictions.

2. PIEZOELECTRIC SHUNTS USING DIGITAL DEVICES

Digital platforms typically work with positive voltage values, between 0V and 5V, whereas piezoelectric materials yields to alternate voltage whose amplitude might exceed hundreds of volts. Figure 1 shows the schematics of a circuit developed to associate piezoelectric elements to digital devices in order to mimic the analog shunts of the traditional piezoelectric-based techniques employed for vibration control. The proposed circuit demands two voltage converters (VC): i) one employed to adjust the piezoelectric voltage to the required input level of the digital device and ii) one to adjust the voltage output of the digital device into the proper voltage level the piezoceramic patches would experience in case they were connected to analog shunts. Note that the voltage converters are not Analog-to-Digital (AD) or Digital-to-Analog (DA) converters. AD-DA converters are considered as elements of the digital platform and the combination of AD-DA converters with the digital processing unit is designated hereafter as digital device.

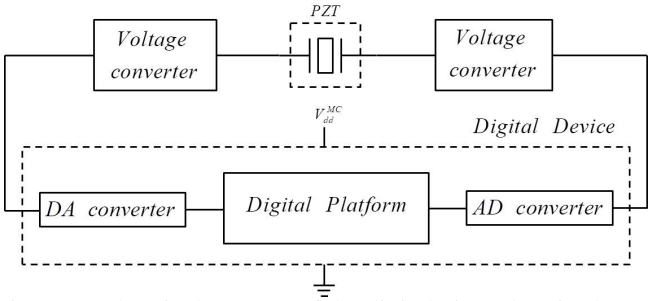

Figure 1: Electrical concept of the digital piezoelectric shunts.

In combination with the two voltage converters (VC), digital devices can create equivalent electrical impedance across the electrodes of a piezoelectric element by establishing a relation between the current (I_p) that flows through the piezoelement and its corresponding voltage (V_p). In the so-called Voltage Based Digital Shunt (VBDS) approach proposed in this paper, such relation is computed by measuring the piezoelectric voltage and calculating the corresponding piezoelectric current, with both tasks being carried out using the digital device. The *input voltage converter*, $\mathrm{VC_{in}}$, (the one that precedes the digital device) performs a weighted sum to enable the digital device to read the electrical output provided by the piezoelectric element (voltage) and the *output voltage converter*, $\mathrm{VC_{out}}$, performs a similar procedure to deliver the signal produced by the digital device back to the piezoelement. Particularly, the first process adds a positive offset to V_p and decreases its amplitude to match the operating range of the digital device, whereas the latter adds a negative offset and increases the amplitude of the output provided by the digital device to properly deliver the electric output to the piezoelement. Figure 2 shows a schematic diagram of the circuitry employed to implement the VBDS approach. One

should notice from the diagram that both voltage converters are each composed of a voltage summing sub-circuit and the difference between $\mathrm{VC_{in}}$ and $\mathrm{VC_{out}}$ is that the first includes the resistor (R_{sh}) and the latter includes the operational amplifier OA1.

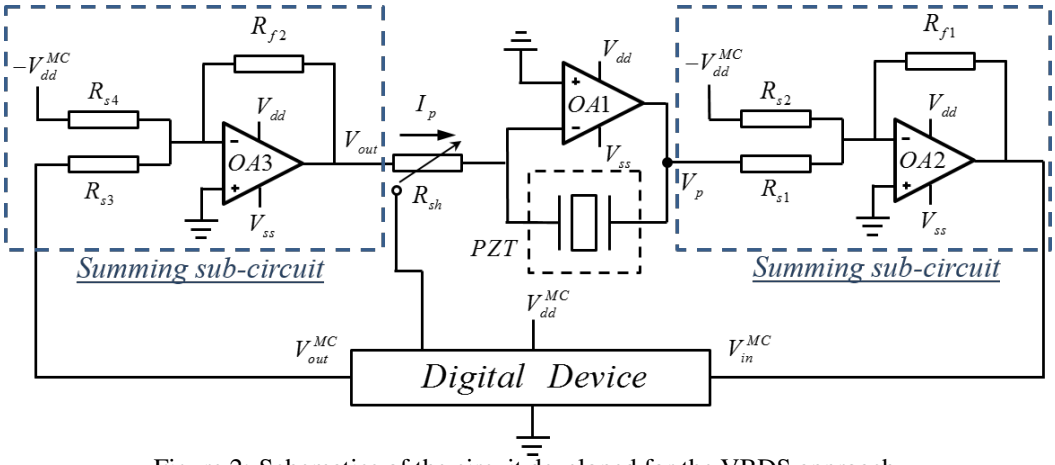

Figure 2: Schematics of the circuit developed for the VBDS approach.

In practical terms, the digital device reads the voltage V_{in}^{MC} that results from the processing of V_p by the *input voltage converter*,

$$V_p = \frac{R_{s1}}{R_{s2}} V_{dd}^{MC} - \frac{R_{s1}}{R_{f1}} V_{in}^{MC}, \tag{1}$$

calculates the correspondent piezoelectric current (I_p) and drives it to the piezoelement after the processing of the *output voltage converter*. The relation between V_p and I_p depends on the vibration control technique employed, as shown in Tab. 1, where the term V_{pi} is used for the switching techniques (SSDS/SSDI) and stands for the piezoelectric voltage value at the beginning of the switch process and ω_d is given by,

$$\omega_d = \sqrt{\frac{1}{LC_p} - \left(\frac{R}{2L}\right)^2}. \tag{2}$$

In the synchronized switch techniques, the piezoceramic patch is switched from the open-circuit condition (where $I_p = 0$) to a specific electric circuit at proper moments. For the digital shunt, the switch action (closed or opened) is obtained by changing the relation between V_p and I_p (which is programmed in the digital device) along time, as described in Tab. 1.

Table 1: Relation between I_p and V_p for different control techniques for the VBDS approach and the corresponding maximum value of I_p.

Linear techniques	**Relation $\mathbf{V_p - I_p}$**		**$\mathbf{\max(I_p)}$**
Resistive	$I_p = \frac{V_p}{R}$		$\frac{\max(V_p)}{R}$
Resistive-inductive in series	$\dot{I}_p = -\frac{R}{L} I_p + \frac{V_p}{L}$		$\frac{\max(V_p)}{\sqrt{R^2+(\omega L)^2}}$
Switched techniques	**Switch close**	**Switch open**	
SSDS	$I_p = \frac{V_{pi}}{R}$	$I_p = 0$	$\frac{\max(V_p)}{R}$
SSDI	$I_p = \frac{1}{L\omega_d} e^{-\frac{R}{2L}t} \sin(\omega_d t)\, V_{pi}$	$I_p = 0$	$\frac{1}{L\omega_d} e^{-\frac{R}{2L}t_m} \sin(\omega_d t_m) \max(V_p)$

After calculating I_p (Tab. 1), the digital device must output an analog voltage (V_{out}^{MC}) that is related to I_p,

$$V_{out}^{MC} = \frac{R_{s3}}{R_{s4}} V_{dd}^{MC} - \frac{R_{s3}}{R_{f2}} R_{sh} I_p, \tag{3}$$

where $R_{sh} = V_{out}/I_p$ is obtained by applying the Ohm's law and V_{out} is the voltage signal after the processing of the *output voltage converter* (Fig. 1). It is important to highlight that since V_{out} is the output voltage of the operational

amplifier *OA*2 (the same condition is valid for V_{in}^{MC} and *OA*3), its maximum value $V_{out} = V_{OpAmp}^{\max}$ is tailored by the supply voltage of the operational amplifier. Hence, the following equation is valid $I_p = \max(I_p)$ (as shown in table 1) and the calculation of R_{sh} is straightforward.

Every technique displayed in Tab. 1 can be employed using the VBDS approach and most part of modifications required to implement the different techniques occur in the digital device programming. That is, no changes are required in the analog part of the circuit except for the resistance R_{sh}, which varies according to the control technique employed. In addition, the resistance values R_{s1}, R_{s2}, R_{s3} and R_{s4} may be obtained from the standard equation of a summing amplifier circuit (Fig. 2). For the *input voltage converter*, for example, one may write eq. 1 as,

$$V_{in}^{MC} = -\frac{R_f}{R_{s1}} V_p + \frac{R_f}{R_{s2}} V_{dd}^{MC}. \tag{4}$$

Assuming $V_{in}^{MC} = max(V_{in}^{MC})$ when $V_p = min(V_p)$ and $V_{in}^{MC} = min(V_{in}^{MC})$ when $V_p = max(V_p)$, hence,

$$max(V_{in}^{MC}) = -\frac{R_f}{R_{s1}} min(V_p) + \frac{R_f}{R_{s2}} V_{dd}^{MC} \tag{5}$$

$$min(V_{in}^{MC}) = -\frac{R_f}{R_{s1}} max(V_p) + \frac{R_f}{R_{s2}} V_{dd}^{MC}. \tag{6}$$

Considering the resistance R_{f1} is selected arbitrarily, one can obtain the resistances R_{s1} and R_{s2} by manipulating eq. 5 and eq. 6 into,

$$R_{s1} = \frac{\Delta V_p}{\Delta V_{in}^{MC}} R_f \tag{7}$$

$$R_{s2} = \frac{\Delta V_p V_{dd}^{MC}}{\Delta V_p max(V_{in}^{MC}) + V_{in}^{MC} min(V_p)} R_f \tag{8}$$

where $\Delta V_p = max(V_p) - min(V_p)$ and $\Delta V_{in}^{MC} = max(V_{in}^{MC}) - min(V_{in}^{MC})$ are design parameters that should be selected according to each application. The same procedure occurs for estimating the resistances R_{s3} and R_{s4} (also, assuming R_{f2} is arbitrarily selected) and, therefore, such derivation shall be omitted.

Moreover, in order to implement the equations that represent the digital shunt circuits into the digital device one must account for the AD-DA converter operations. In this sense, the analog voltage read by the digital device, is linearly converted to discrete levels as shown in Fig. 3(a), where $L = 2^n - 1$, n is the number of bits of the AD converter and the parameters $min\left(V_{in}^{MC}\right)$, $max\left(V_{in}^{MC}\right)$ and L are assumed to be known. Hence, the relation between the analog voltage measured and the level digitally obtained is written as $V_{in}^{MC} = al + b$, where $a = \left(max\left(V_{in}^{MC}\right) - min\left(V_{in}^{MC}\right)\right)/L$ and $b = min\left(V_{in}^{MC}\right)$. A similar procedure occurs for the analog output generated by the digital device, whereas the level is $l = c\, V_{out}^{MC} + d$ (Fig. 3(b)) and the constants are $c = L/\Delta V_{out}^{MC}$ and $d = -\left(L\ min\left(V_{out}^{MC}\right)\right)/\Delta V_{out}^{MC}$.

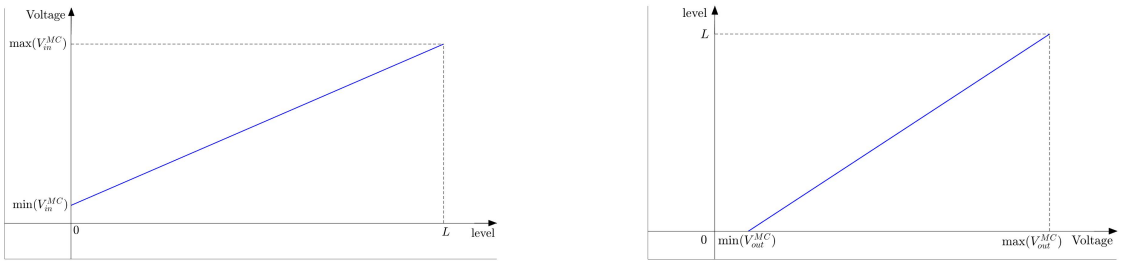

(a) (b)

Figure 3: Relation between discrete level and analog voltage of the digital device at its (a) input and (b) output.

Therefore, using the correction factors (a,b,c and d) and rearranging eq. 1 and eq. 3 into a more compact for one should obtain the correct form to implement the digital shunt equations:

$$V_p = \bar{A}_1 L + \bar{A}_2 \tag{9}$$

$$l = \bar{A}_3 \left(V_{p1} + R_{meas} I_{p1}\right) + \bar{A}_4 \tag{10}$$

$$\bar{A}_1 = A_1\, a,\ \bar{A}_2 = A_1\, b + A_2,\ \bar{A}_3 = A_3\, c \text{ and } \bar{A}_4 = A_4\, c + d \tag{11}$$

$$A_1 = \quad -\frac{R_{s1}}{R_{f1}}, \qquad A_2 = \frac{R_{s1}}{R_{s2}} V_{dd}^{MC} \tag{12}$$

$$A_3 = \quad -\frac{R_{s3}}{R_{f2}} R_{sh}, \quad A_4 = \frac{R_{s3}}{R_{s4}} V_{dd}^{MC}. \tag{13}$$

3. NUMERICAL RESULTS AND EXPERIMENTAL VERIFICATION

This section presents the numerical results obtained for the VBDS approach, as well as the experimental verification performed for the proposed digital shunts. Simulations were performed using the Matlab-Simulink block diagram shown in Fig. 4(b) for a linear electromechanically coupled structure (Fig. 4(a)) governed by

$$m\ddot{x} + c\dot{x} + kx - \theta V_p = F_e \tag{14}$$

$$C_p V_p + Q_p + \theta x = 0. \tag{15}$$

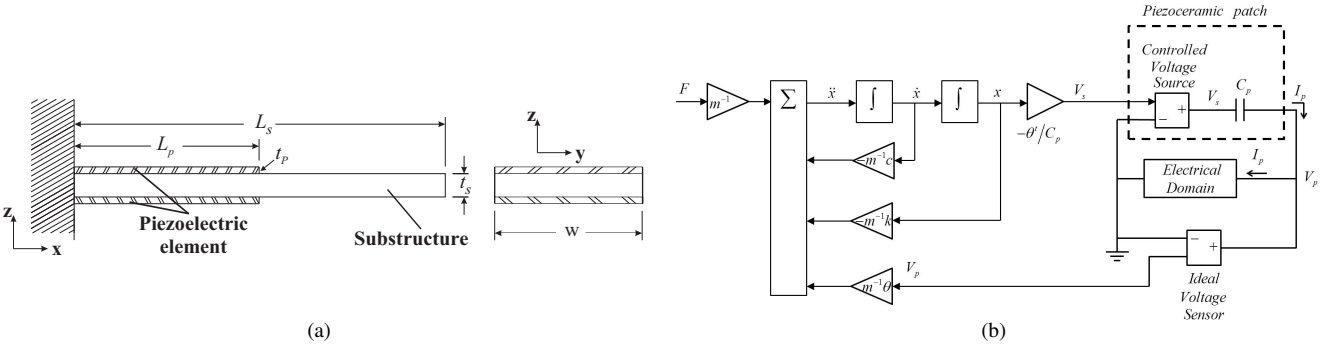

Figure 4: Schematics of (a) a generic piezoelectric beam structure and (b) its block diagram equivalent model.

The linear electromechanically coupled structure considered here is an aluminum cantilever beam with two piezoelectric patches (PZT5A) attached to the upper and lower surface of the host structure, as illustrates the schematics presented in Fig. 4(a), where L_s is the length of the substrate, L_p is the length of the piezoelectric element, t_p is the thickness of the piezoelement, t_s is the thickness of the substrate and w is the width of both the piezoelement and substrate. The piezoelectric elements were connected in parallel (which yields to an equivalent piezoelectric capacitance of 106nF) and a tip mass of 22.9g was considered. The simulations were carried out using the Rayleight-Ritz approximations considering the first 10 mode-shapes of the structure and an harmonic base excitation. Table 2 shows the dimensions and properties of the structure.

Table 2: Geometrical and material properties of the aluminum beam and PZT5A.

Aluminum beam	Value	Properties PZT5A	Value
Length (mm)	115.60	Length (mm)	36.10
Width (mm)	27.80	Width (mm)	20.57
Thickness (mm)	1.02	Thickness (mm)	0.24
Young's Modulus (Gpa)	70.00	Young's Modulus (Gpa)	67.00
Density (kg/m^3)	2700.00	Density (kg/m^3)	7750.00
ϵ	1800.00	Piezoelectric constant d_{31} (pm/V)	-171.00

In Fig. 4(b), the block "Electrical Domain" can simulate the digital shunts proposed in this paper as well as different analog circuits. For example, it is possible to simulate the a resistive circuit by inserting an analog resistor inside the "Electrical Domain" block or by inserting the digital shunts circuitry. If all the equations and circuitry of the digital shunt are correctly implemented, both cases must yield to the same mechanical (x, $\dot{x}$ and $\ddot{x}$) and electrical (V_p and Q_p) outputs for the electromechanically coupled structure, thus numerically validating the digital shunts. The electrical components used in the numerical simulations and experimental verification for the VBDS approach are exhibited in Tab. 3.

The experimental procedure was carried out for the same conditions simulated numerically (boundary condition, excitation amplitude and frequency bandwidth), i.e. considering the same electromechanically coupled structure (Tab. 2)

Table 3: Electrical components of the VBDS circuit.

Parameter	Value	Parameter	Value
R_{s1}	1.11MΩ	R_{s2}	303.03kΩ
R_{s3}	7.50kΩ	R_{s4}	23.43kΩ
R_{f1}	100.00kΩ	R_{f2}	100.00kΩ
$OA1$,$OA2$,$OA3$	LM358	MCU	Arduino Due 2009

and circuit parameters. A MT 160 shaker (manufactured by Labworks Inc.) driven by PA 138 linear power amplifier (manufactured by Labworks Inc.) and a LMS-Siemens SCADAS is responsible for the excitation force, whereas a low-mass accelerometer (model PCB352A24) fixed at the clamp monitores the base acceleration and a Polytec PDV 100 laser Doppler vibrometer measures the beam tip velocity. An U8031A 0-30 V DC power supply (manufactured by Keysight Technologies) powers active components of the circuitry. The mechanical tip velocity ($\dot{x}$) and electrical outputs (V_p) of the system were recorded using the LMS-Siemens SCADAS system. Figure 5 depicts all the equipment employed during the experimental tests.

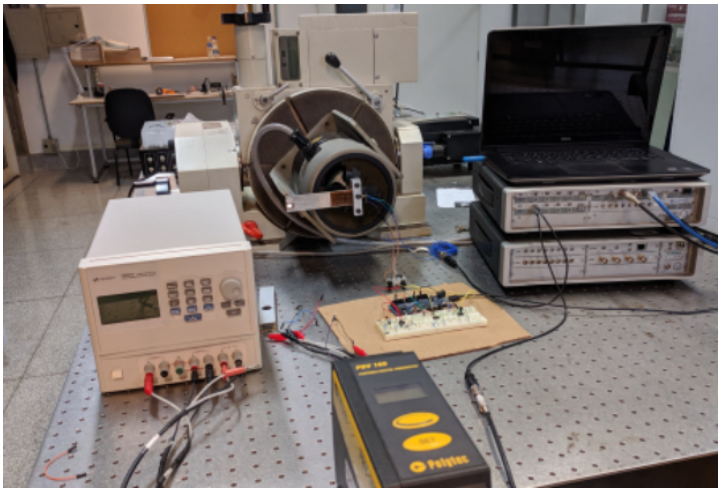

Figure 5: Equipment setup used during the experimental tests.

Results are shown as Frequency Response Function (FRF) of the beam tip velocity and the piezoelectric voltage per base acceleration for the linear cases (resistive and resistive-inductive in series), whereas for the nonlinear cases (SSDS, SSDI and NES) the frequency spectra analyzed for the same output signals resulted from a closed-loop stepped-sine base excitation. As it can be seen from Fig. 6 and Fig. 7, in a general sense there is good agreement between numerical and experimental results of the VBDS, CBDS and the baseline analog correspondent cases for all circuits analyzed.

For the RLs results (Fig. 6(a), Fig. 6(b), Fig. 7(a) and Fig. 7(b)) the resistance value of 500Ω represents the near purely inductive case, the $10M\Omega$ resistance represents the near open-circuit condition and the $10k\Omega$ resistance represents the optimal value to reduce vibrations since the FRF exhibits a charateristic plateau-like curve as reported in the literature. An inductance sweep was (numerically) performed in the vicinity of the value $L = 1/\omega_n^2 C_p$ in order to obtain the optimal inductance $L = 0.93/\omega_n^2 C_p$. It is important to mention that employing the VBDS technique to reproduce the RLs technique present a great advantage in practical applications when compared to the analog approach. For the presented case (Fig. 6(b)), for example, the required inductance, $352H$, would demand a very large coil, which would be impractical in many applications. However, the digital approach can simulate a $352H$ inductor (and even higher inductance values) with the advantage of enabling the internal resistance of the inductance to be adjusted accordingly, meaning that very high quality factor inductors can be obtained.

The SSDS/SSDI results (Fig. 6(c), Fig. 6(d), Fig. 7(c) and Fig. 7(d)) were obtained when the system was excited near its first resonance frequency at a base acceleration level of 0.04g. In the SSDS case, it is considered that the piezoelectric patch is switched to a resistance load of $5k\Omega$ and, in the SSDI case, the piezoceramic patch is switched to an inductor of $1.96H$ with an internal resistance of $2k\Omega$. In both cases, an ideal switch (with no internal resistance or threshold to be triggered) is considered and the switch is closed precisely at the voltage extrema. Such characteristic is not commonly obtained with analog shunts but it can be easily implemented in digital shunts, providing better control on the internal resistance as well as switching moments, thus, allowing the inversion the process to occur with very low losses and consequently increase the performance of the technique. It is noteworthy mentioning that the results shown in Fig. 6(c)

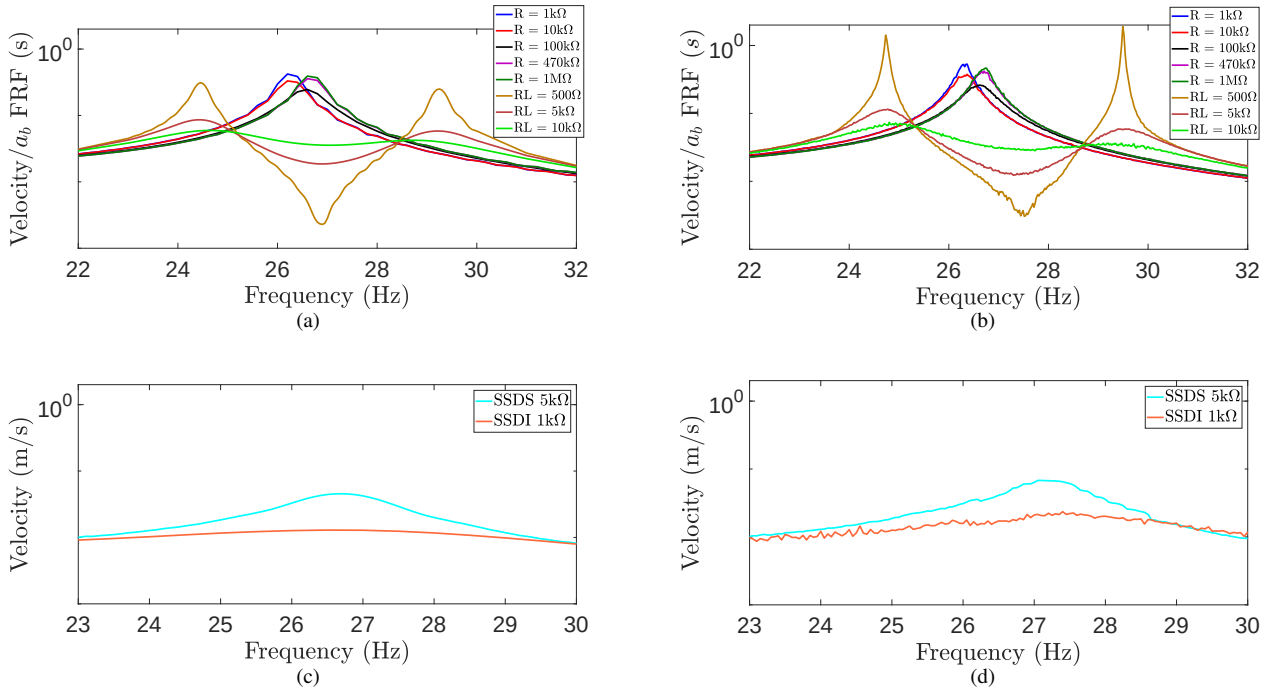

Figure 6: Comparison of numerical and experimental results for the (a-b) tip velocity FRF regarding the linear techniques and (c-d) the tip velocity spectrum for the nonlinear switching techniques.

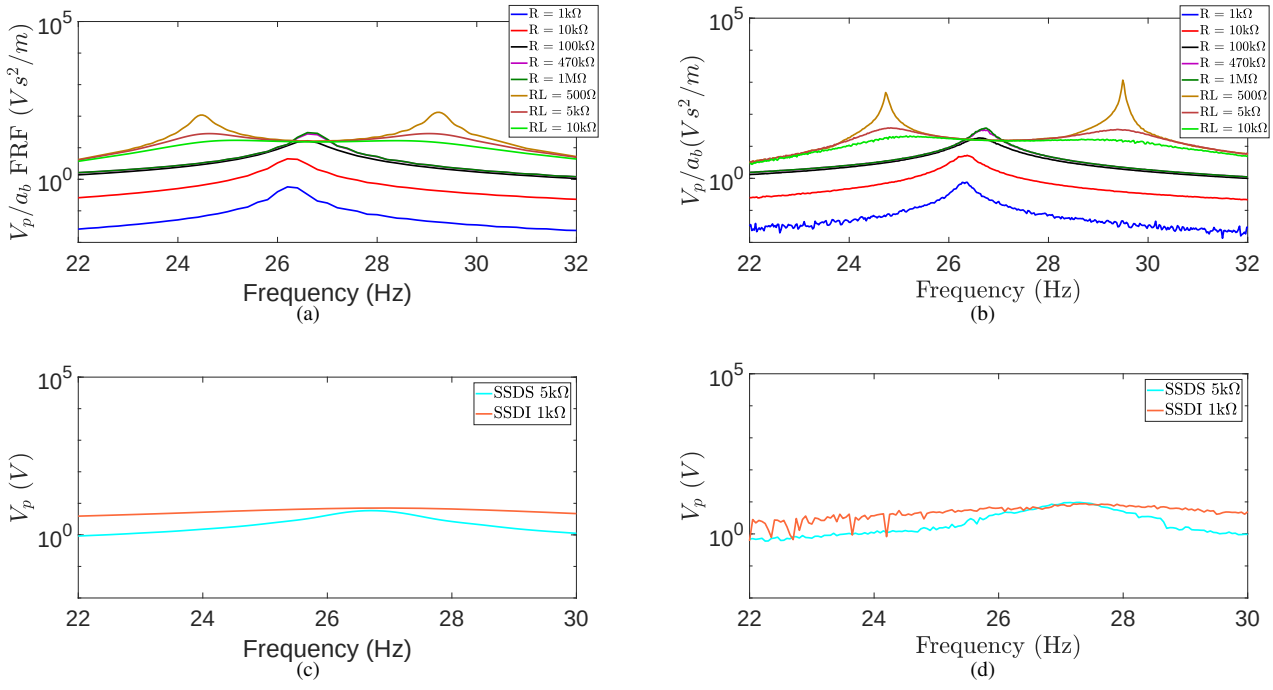

Figure 7: Comparison of numerical and experimental results for the (a-b) voltage FRF regarding the linear techniques and (c-d) the voltage spectrum for the nonlinear switching techniques.

are obtained when the electromechanical coupling of the first mode is considered. The presence of higher harmonics undermine the performance of the SSDS/SSDI technique to detect the piezoelectric voltage extrema originating from the first mode.

4. CONCLUSIONS

This paper presents an approach to implement digital shunt for different piezoelectric-based vibration control techniques presented in the literature. The proposed digital shunt (VBDS) can successfully reproduce the linear resistive and resistive-inductive techniques as well as the SSDS/SSDI nonlinear switching techniques. On the other hand, the VBDS cannot handle polynomial relations between I_p and V_p and therefore is not able to implement polynomial nonlinear techniques such as the Nonlinear Energy Sink. This issue is being addressed and on going work is currently being done to development another digital shunt circuit.

5. ACKNOWLEDGEMENTS

The authors would like to thank the São Paulo Research Foundation (FAPESP - São Paulo, Brazil) [grant number 99999.003755/2015-00] and the National Council for Scientific and Technological Development (CNPq) [grant numbers 380603/2019-5 and 433456/2018-3] for the financial support.

6. REFERENCES

Clark, W.W., 2000. "Vibration Control with State-Switched Piezoelectric Materials". *Journal of Intelligent Material Systems and Structures*, Vol. 11, No. 4, pp. 263–271. ISSN 1045389X. doi:10.1106/18CE-77K4-DYMG-RKBB.

Corr, L.R. and Clark, W.W., 2002. "Comparison of low-frequency piezoelectric switching shunt techniques for structural damping". *Smart Materials and Structures*, Vol. 11, No. 3, pp. 370–376. ISSN 09641726. doi:10.1088/0964-1726/11/3/307.

Forward, R.L., 1979. "Electronic damping of vibrations in optical structures". *Applied Optics*, Vol. 18, No. 5, p. 690. ISSN 0003-6935. doi:10.1364/AO.18.000690.

Guyomar, D., Richard, C., Gehin, C. and Audigier, D., 2000. "Low consumption damping of planar structures". In *ISAF 2000. Proceedings of the 2000 12th IEEE International Symposium on Applications of Ferroelectrics (IEEE Cat. No.00CH37076)*. IEEE, Vol. 2, pp. 761–764. ISBN 0-7803-5940-2. doi:10.1109/ISAF.2000.942431.

Hagood, N. and Von Flotow, A., 1991. "Damping of structural vibrations with piezoelectric materials and passive electrical networks". *Journal of Sound and Vibration*, Vol. 146, pp. 243–268.

Lesieutre, G.A., 1998. "Vibration damping and control using shunted piezoelectric materials". *Shock and Vibration Digest*, Vol. 30, No. 3, pp. 187–195.

Lossouarn, B., Deü, J.F. and Kerschen, G., 2018. "A fully passive nonlinear piezoelectric vibration absorber". *Philosophical Transactions of the Royal Society A: Mathematical, Physical and Engineering Sciences*, Vol. 376, No. 2127, p. 20170142. ISSN 1364-503X. doi:10.1098/rsta.2017.0142.

Matten, G., Collet, M., Cogan, S. and Sadoulet-Reboul, E., 2014. "Synthetic Impedance for Adaptive Piezoelectric Metacomposite". *Procedia Technology*, Vol. 15, pp. 84–89. ISSN 22120173. doi:10.1016/j.protcy.2014.09.037. URL `http://linkinghub.elsevier.com/retrieve/pii/S2212017314001522`.

Moheimani S.O.R., 2003. "A survey of recent innovations in vibration damping and control using shunted piezoelectric transducers". *IEEE Transactions on control systems technology*, Vol. 11, No. 4, pp. 482–494.

Nečásek, J., Václavík, J. and Marton, P., 2016. "Digital synthetic impedance for application in vibration damping". *Review of Scientific Instruments*, Vol. 87, No. 2, p. 024704. ISSN 0034-6748. doi:10.1063/1.4942085. URL `http://aip.scitation.org/doi/10.1063/1.4942085`.

Richard, C., Guyomar, D., Audigier, D. and Bassaler, H., 2000. "Enhanced semi passive damping using continuous switching of a piezoelectric device on an inductor ." In T.T. Hyde, ed., *Proc. SPIE 3989, Smart Structures and Materials 2000: Damping and Isolation*. Vol. 3989, pp. 288–299. doi:10.1117/12.384569.

Richard, C., Guyomar, D., Audigier, D. and Ching, G., 1999. "Semi-passive damping using continuous switching of a piezoelectric device". In T.T. Hyde, ed., *Proc. of SPIE 3672, Smart Structures and Materials 1999: Passive Damping and Isolation*. Newport Beach, CA, Vol. 3672, pp. 104–111. doi:10.1117/12.349773.

Uchino, K. and Ishii, T., 1988. "Mechanical Damper Using Piezoelectric Ceramics". *Journal of the Ceramic Society of Japan*, Vol. 96, No. 1116, pp. 863–867. ISSN 1882-1022. doi:10.2109/jcersj.96.863.

Wu, S.y., 1996. "Piezoelectric shunts with a parallel R-L circuit for structural damping and vibration control". In C.D. Johnson, ed., *Proc. SPIE 2720, Smart Structures and Materials: Passive Damping and Isolation*. Vol. 27201259, pp. 259–269. ISBN 0819420956. doi:10.1117/12.239093.

7. RESPONSIBILITY NOTICE

The following text, properly adapted to the number of authors, must be included in the last section of the paper:
The author(s) is (are) the only responsible for the printed material included in this paper.